Proteus mirabilis fimbriae- and urease-dependent clusters assemble in an extracellular niche to initiate bladder stone formation

Jessica N. Schaffer[a,1], Allison N. Norsworthy[a,1], Tung-Tien Sun[b,c,d,e], and Melanie M. Pearson[a,e,2]

[a]Department of Microbiology, New York University Medical Center, New York, NY 10016; [b]Department of Cell Biology, New York University Medical Center, New York, NY 10016; [c]Department of Dermatology, New York University Medical Center, New York, NY 10016; [d]Department of Biochemistry and Molecular Pharmacology, New York University Medical Center, New York, NY 10016; and [e]Department of Urology, New York University Medical Center, New York, NY 10016

Edited by Scott J. Hultgren, Washington University School of Medicine, St. Louis, MO, and approved March 8, 2016 (received for review February 3, 2016)

The catheter-associated uropathogen *Proteus mirabilis* frequently causes urinary stones, but little has been known about the initial stages of bladder colonization and stone formation. We found that *P. mirabilis* rapidly invades the bladder urothelium, but generally fails to establish an intracellular niche. Instead, it forms extracellular clusters in the bladder lumen, which form foci of mineral deposition consistent with development of urinary stones. These clusters elicit a robust neutrophil response, and we present evidence of neutrophil extracellular trap generation during experimental urinary tract infection. We identified two virulence factors required for cluster development: urease, which is required for urolithiasis, and mannose-resistant *Proteus*-like fimbriae. The extracellular cluster formation by *P. mirabilis* stands in direct contrast to uropathogenic *Escherichia coli*, which readily formed intracellular bacterial communities but not luminal clusters or urinary stones. We propose that extracellular clusters are a key mechanism of *P. mirabilis* survival and virulence in the bladder.

Proteus mirabilis | urinary tract infection | urease | fimbriae | bladder stones

The pathogen *Proteus mirabilis* is linked with catheter-associated urinary tract infections (UTIs), where it can cause complications including crystalline biofilms, urinary stones, pyelonephritis, and septicemia (1–3). Although numerous studies have identified aspects of *P. mirabilis* biology that are important for infection, the *P. mirabilis* pathogenic life cycle is poorly understood. Moreover, we lack a mechanistic understanding of the contributions of essential virulence factors. For example, although mannose-resistant *Proteus*-like (MR/P) fimbriae are required to maximally colonize the bladder and kidneys and are important for hemagglutination, biofilm formation, and autoaggregation in vitro, their binding target and in vivo role remain elusive (4–6).

Visualization of *P. mirabilis* in experimentally infected mice at 48 h postinfection (hpi) and beyond found *P. mirabilis* in the urinary tract individually, in groups, and embedded in urinary stones (5, 7–9). Urolithiasis, the process of stone formation, requires urease, which releases ammonia and increases urinary pH via urea hydrolysis, resulting in the precipitation of calcium and magnesium compounds into urinary stones (10, 11). However, early stages in stone development remained unobserved in vivo, and it was unclear how this process was connected to early events in colonization and pathogenesis.

The early colonization events of uropathogenic *Escherichia coli* (UPEC), a major cause of uncomplicated UTI, have been delineated. Upon bladder entry, UPEC attaches to superficial urothelial cells (umbrella cells) that line the bladder lumen (12). The apical surface of umbrella cells is covered in 2D crystalline plaques formed by heterotetramers of four uroplakin proteins (UPIa, UPIb, UPII, and UPIIIa) (13). UPEC adheres to UPIa on the apical surface with type 1 fimbriae, which triggers the uptake of UPEC by umbrella cells (12). Once inside umbrella cells, UPEC can multiply and form organized groups of tightly packed bacteria known as intracellular bacterial communities (IBCs) (14). These IBCs may completely fill the umbrella cell before the cell either ruptures or is exfoliated, causing a rapid increase in umbrella cell turnover (14–16). In addition to intracellular replication, UPEC can multiply extracellularly in the bladder lumen, reaching up to 10^7 colony forming units (cfu)/mL (17, 18).

In this study, we compare the initial events of *P. mirabilis* bladder infection with the well-established life cycle of UPEC. Although initial attachment and invasion of *P. mirabilis* resembles that of UPEC, *P. mirabilis* forms IBCs that are significantly rarer and smaller than UPEC IBCs. Instead, the majority of *P. mirabilis* bacteria are in large, extracellular clusters in the bladder lumen. These clusters promote extensive neutrophil infiltration and deposition of calcium ions, a crucial initial step in urolithiasis. Importantly, cluster development requires both MR/P fimbriae and urease. This work elucidates a *P. mirabilis* life style that is distinct from UPEC's and uncovers functions for two critical virulence factors in infection.

Results

***P. mirabilis* Rapidly Invades the Urothelium but Rarely Establishes IBCs.** Previous studies of *P. mirabilis* pathogenesis did not document events within the first 24 h of infection. To investigate the in vivo localization of *P. mirabilis* during the early stages of pathogenesis, we visualized bacteria and the urothelial surface—defined by UPIIIa staining—in sections of infected murine bladders during the first 24 hpi. We found that *P. mirabilis* attached to the urothelial surface by 0.5 hpi. In some instances, *P. mirabilis* and UPIIIa staining overlapped, suggesting that *P. mirabilis* may invade the urothelium within this time frame (Fig. 1*A*). However, we infrequently observed intracellular bacteria at later time points; although *P. mirabilis* formed IBCs at 6, 10, and 24 hpi (Fig. 1*A*), IBCs were rare (Table 1 and Fig. 1*B*) and small (Fig. 1*G*).

Significance

Early events during *Proteus mirabilis*-mediated urinary tract infection have not been well defined. Here we demonstrate that, in contrast to uropathogenic *Escherichia coli*, *P. mirabilis* rarely forms bladder intracellular communities. Rather, in the bladder lumen it establishes large urease- and mannose-resistant *Proteus*-like fimbriae-dependent clusters, which draw a massive neutrophil response and are precursors to urinary stones.

Author contributions: J.N.S., A.N.N., T.-T.S., and M.M.P. designed research; J.N.S. and A.N.N. performed research; J.N.S. contributed new reagents/analytic tools; J.N.S., A.N.N., T.-T.S., and M.M.P. analyzed data; and J.N.S., A.N.N., and M.M.P. wrote the paper.

The authors declare no conflict of interest.

This article is a PNAS Direct Submission.

[1]J.N.S. and A.N.N. contributed equally to this work.

[2]To whom correspondence should be addressed. Email: melanie.pearson@nyumc.org.

This article contains supporting information online at www.pnas.org/lookup/suppl/doi:10.1073/pnas.1601720113/-/DCSupplemental.

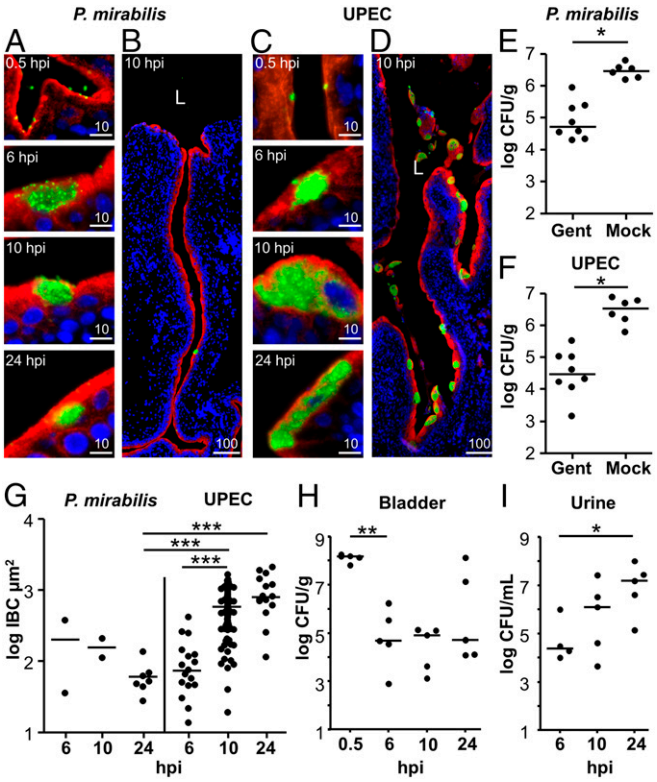

Fig. 1. *P. mirabilis* invades the urothelium, but infrequently forms IBCs. (*A–D*) Representative images of *P. mirabilis* (*A* and *B*) and UPEC (*C* and *D*) attachment and invasion. Bacteria (green), UPIIIa (red), and DNA (blue) show localization of the bacteria relative to the apical surface of the urothelium. (Scale bars, 10 μm.) (*B* and *D*) A regional view of the bladder section containing the 10 hpi IBC shown in *A* and *C*, respectively. (Scale bars, 100 μm.) L, bladder lumen. (*E* and *F*) Quantification of *P. mirabilis* (*E*) and UPEC (*F*) bladder invasion at 0.5 hpi following either ex vivo gentamicin treatment (Gent) or mock treatment (Mock) ($n = 6–8$). *$P < 0.05$. (*G*) Size of *P. mirabilis* and UPEC IBCs. Every observed IBC was measured from *P. mirabilis*-infected sections, as well as from UPEC-infected sections at 6 and 24 hpi. However, due to the high number of IBCs in UPEC-infected mice at 10 hpi, sizes were determined from two sections, each from a different mouse. See Table 1 for details on the IBC frequency relative to the number of sections and mice. (*H* and *I*) Quantification of the cfu detected during *P. mirabilis* infection of the bladder (*H*) and urine (*I*). Each data point represents an individual animal.

As a comparison, we examined UPEC in our model system. UPEC also attached to and appeared to invade the urothelial surface by 0.5 hpi (Fig. 1*C*). By 6 hpi, most detected bacteria were intracellular (Fig. 1*C*). At 10 hpi, IBCs were larger and more abundant, and the bladder lumen contained shed epithelial cells with IBCs (Fig. 1 *C* and *D*). Finally, at 24 hpi, we observed a decrease in the number of IBCs, consistent with the exfoliation of epithelial cells containing IBCs (Table 1). Notably, UPEC IBCs at 10 and 24 hpi were significantly larger than *P. mirabilis* IBCs at their most abundant time point (Fig. 1*G*, 24 hpi).

Because we observed evidence of invasion, we used an ex vivo gentamicin protection assay to enumerate intracellular bacteria. Both *P. mirabilis* and UPEC invaded the bladder urothelium by 0.5 hpi, as shown by a significant difference between gentamicin- and mock-treated bladders ($P = 0.0107$ and 0.0194, respectively), and both bacterial species had a similar amount of invasion (5.3×10^4 and 3.0×10^4 cfu/g tissue, respectively) (Fig. 1 *E* and *F*). When bladders were homogenized before gentamicin treatment, we rarely detected viable bacteria, indicating that gentamicin treatment effectively kills accessible bacteria (Fig. S1).

To assess bacterial colonization over time, we enumerated the total *P. mirabilis* load in murine bladders at 0.5, 6, 10, and 24 hpi (Fig. 1*H*). At 0.5 hpi, infection was tightly clustered at a median of 1.5×10^8 cfu/g bladder. By 6 hpi, the bacterial burden decreased significantly to an average of 4.8×10^4 cfu/g bladder ($P = 0.0079$), whereas the variability in bacterial burden increased (Fig. 1*H*). Between 6 and 24 hpi the bacterial burden in the urine ($P = 0.0317$), but not in the bladder tissue, increased significantly (Fig. 1*I*). Individual mice with higher bladder bacterial burdens emerged at 24 hpi, suggesting the beginning of divergent disease courses (Fig. 1*H*). Notably, we observed differences in the bacterial load when bladders were homogenized immediately (1.5×10^8 cfu/g) (Fig. 1*H*) versus when they were homogenized after mock treatment and washes (2.9×10^6 cfu/g) (Fig. 1*E*), suggesting that at this early time point a large proportion of *P. mirabilis* weakly associate with the bladder surface.

***P. mirabilis* Forms Large Extracellular Clusters in the Bladder Lumen.** Remarkably, although *P. mirabilis* was difficult to detect using microscopy at 6 hpi, by 24 hpi *P. mirabilis* formed large extracellular clusters (median 5.9×10^4 μm², $n = 6$) (Fig. S2) in the bladder lumen of the majority (five of seven) of infected mice (Fig. 2 *A* and *C*). Mice at 10 hpi displayed an intermediate phenotype with clusters detected in two of seven mice (Fig. 2 *B* and *C*). Generally, clusters were directly adjacent to the bladder surface, associated with urothelial destruction (as shown by minimal surface-associated uroplakin staining adjacent to the cluster), and had a large, unusual region of dense DAPI staining near the cluster. However, at both 10 hpi (Fig. 2*B*) and 24 hpi (Fig. S3), one of the detected clusters was unattached to the urothelium, showed limited urothelial damage, and had normal DAPI staining. We suspect that these two clusters represent either early stages of cluster formation or successful disruption of cluster development by the host. Clusters were rarely observed in voided urine (Fig. S4). Because the formation of these exceptionally large luminal bacterial clusters during UTI was an intriguing finding, we focused further studies on this phenotype.

***P. mirabilis* Extracellular Clusters Are an Early Stage of Urolithiasis.** A classic characteristic of *P. mirabilis* UTI is the development of urinary stones. Although mature stones have been imaged, early stones were undocumented in vivo (11). We hypothesized that concentrated urease activity within clusters would cause localized deposition of struvite and carbonate apatite. To test this hypothesis, we used Alizarin Red staining, which primarily detects calcium salts, but can also detect magnesium and other minerals (8). In support of our hypothesis, Alizarin Red strongly stained sections of *P. mirabilis*-infected bladders that contained extracellular clusters at 24 hpi (Fig. 2*D*). Conversely, *P. mirabilis*-infected bladders without clusters, regardless of the timing, were unstained by Alizarin Red (Fig. 2*D*). As expected, because UPEC does not produce urease, sections of highly infected bladders with many IBCs remained Alizarin Red-negative (Fig. 2*E*). These data support our hypothesis that *P. mirabilis* clusters result in mineral deposition that serves as an early step in stone formation.

***P. mirabilis* Extracellular Clusters Induce an Extensive Neutrophil Response.** We reasoned that a large cluster of *P. mirabilis* cells associated with epithelial destruction in the bladder would induce a potent immune response; furthermore, neutrophil influx is critical for clearance of UPEC bladder infection (19). In support of this, we

Table 1. Quantification of IBCs in infected bladders

	P. mirabilis			UPEC		
Observations	6 hpi	10 hpi	24 hpi	6 hpi	10 hpi	24 hpi
IBCs	2	2	7	17	337	20
Sections examined	16	34	39	10	9	11
Mice with IBCs	1	1	2	2	2	2
Mice with clusters	0	2	5	0	0	0
Total mice	4	7	7	3	2	2

MICROBIOLOGY

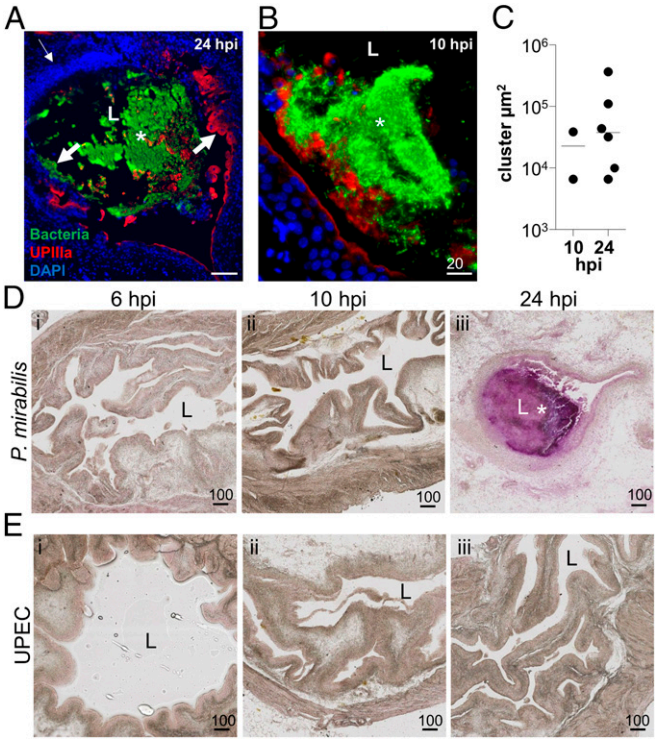

Fig. 2. *P. mirabilis* extracellular clusters are precursors to stone formation. (*A* and *B*) A representative image of a *P. mirabilis* cluster at 24 hpi (*A*). (Scale bar, 100 μm.) (*B*) A *P. mirabilis* cluster at 10 hpi with limited urothelial destruction and normal DAPI staining. (Scale bar, 20 μm.) In both *A* and *B*, staining of bacteria (green), UPIIIa (red), and DNA (blue) show accumulation of bacterial clusters at the bacteria–bladder interface. An asterisk indicates an extracellular cluster; L, bladder lumen. The thin arrow indicates a region with increased DAPI signal, whereas thick arrows indicate areas of extensive urothelial damage. (*C*) Area of every extracellular cluster detected in *P. mirabilis*-infected murine bladders ($n = 7$ mice each at 10 and 24 hpi). (*D* and *E*) Detection of mineral deposition using Alizarin Red staining of (*D*) *P. mirabilis*- and (*E*) UPEC-infected bladder sections at (*i*) 6, (*ii*) 10, and (*iii*) 24 hpi. (Scale bars, 100 μm.) L, bladder lumen; an asterisk indicates extracellular cluster (purple staining).

often observed ($n = 5$ of 6 clusters) a large mass of DAPI staining adjacent to *P. mirabilis* extracellular clusters at 24 hpi (Fig. 2*A*), which also stained positive for the surface-expressed, neutrophil-specific marker Ly6G (20, 21), in the densely stained DAPI region adjacent to bacterial clusters. We detected three unique patterns of Ly6G/DAPI staining in areas near clusters: $Ly6G^+DAPI^+$ (Fig. 3*A*), $Ly6G^+DAPI^-$ (Fig. 3 *A* and *B*), and $Ly6G^-DAPI^+$ (Fig. 3*B*). We hypothesized that $Ly6G^+DAPI^-$ and $Ly6G^-DAPI^+$ regions may represent neutrophil extracellular traps (NETs)—extracellular webs of DNA covered in antimicrobial peptides and proteins released by the neutrophil cell body—that trap and kill pathogens (22). To identify NETs, we stained for H2A, a histone marker that remains attached to eukaryotic DNA during NETosis, the process of NET formation (22, 23). Indeed, we observed colocalization of H2A and DAPI in areas adjacent to $Ly6G^+$ staining (Fig. 3 *B* and *C*). Upon magnification, we observed a fiber-like pattern of overlapping H2A and DAPI staining independent of the membrane Ly6G staining, indicative of NET formation (Fig. 3*C*). The degree of separation between nuclear contents ($H2A^+DAPI^+$) and the membrane staining ($Ly6G^+$) suggests that neutrophils may be undergoing vital NETosis, in which neutrophils continue to function as anuclear cytoplasts after NET expulsion (24, 25). We also observed a NET-like mass of neutrophils and epithelial cells in the urine of one mouse (Fig. S4*B*). Finally, we reasoned that $Ly6G^+DAPI^+$ regions could represent intact neutrophils: indeed, some of the $Ly6G^+DAPI^+$ cells appeared to have phagocytosed bacteria, a prototypical function of these innate immune cells (Fig. 3*D*).

As a comparison, we assessed neutrophil influx in *P. mirabilis*-infected bladders in cluster-distal regions, as well as in UPEC-infected bladders. For UPEC, we found only individual, apparently intact neutrophils in the vicinity of bacteria, including IBCs, at 10 and 24 hpi (Fig. 3*E*). We saw a similar phenotype in regions of *P. mirabilis*-infected bladders distant from clusters at 10 and 24 hpi (Fig. 3*E*). We did not detect neutrophils in naive bladders, consistent with other reports (26, 27). Taken together, these data suggest that *P. mirabilis* clusters elicit a specific immune response that is robust and distinct from UPEC.

Formation of *P. mirabilis* Extracellular Clusters Requires Both MR/P Fimbriae and Urease. We next sought to identify bacterial factors that mediate cluster formation. Because our evidence suggested that these clusters are a precursor to stone formation, we compared the phenotype of a urease-negative *P. mirabilis ureC* mutant to the wild-type parent at 24 hpi. As expected, clusters in wild-type infected bladders detected by immunofluorescence closely corresponded with Alizarin Red-positive regions (Fig. 4*A*). In contrast, we did not observe Alizarin Red staining or extracellular clusters in sections from mice infected with the *ureC* mutant ($n = 5$) (Fig. 4*B*). Instead, bacteria were rarely observed and primarily in small intracellular groups (Fig. 4*B*). These results indicate that urease is important for the formation and/or

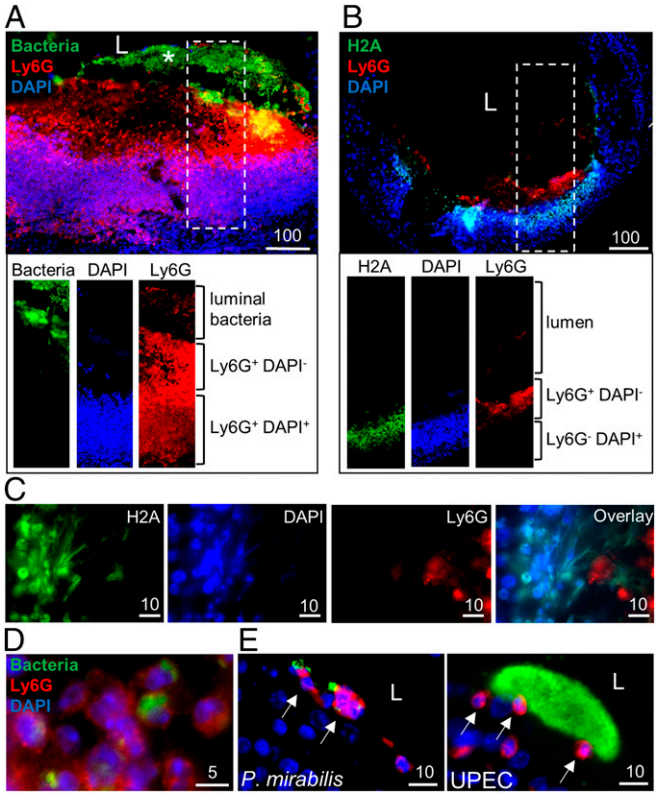

Fig. 3. *P. mirabilis* induces neutrophil recruitment and NET formation. (*A* and *B*) Visualization of neutrophil recruitment at extracellular clusters at 24 hpi. Individual channels for the region enclosed in the dashed rectangle are shown below at the same magnification. (Scale bars, 100 μm.) (*C*) Identification of NET formation in regions of neutrophil recruitment at 24 hpi. Individual channels representing nuclear stains (H2A and DAPI) and membrane stains (Ly6G) show the overlap of DAPI and H2A distant from Ly6G staining. (Scale bars, 10 μm.) (*D*) Neutrophil phagocytosis of *P. mirabilis* at 24 hpi. Arrows indicate neutrophils which have phagocytosed bacteria. (*E*) Individual neutrophil recruitment in sections of murine bladders infected with *P. mirabilis* without clusters at 24 hpi and UPEC-infected sections at 10 hpi. Bacteria (green), Ly6G (red), and DNA (blue) show neutrophils adjacent to bacteria. Arrows indicate intact neutrophils.

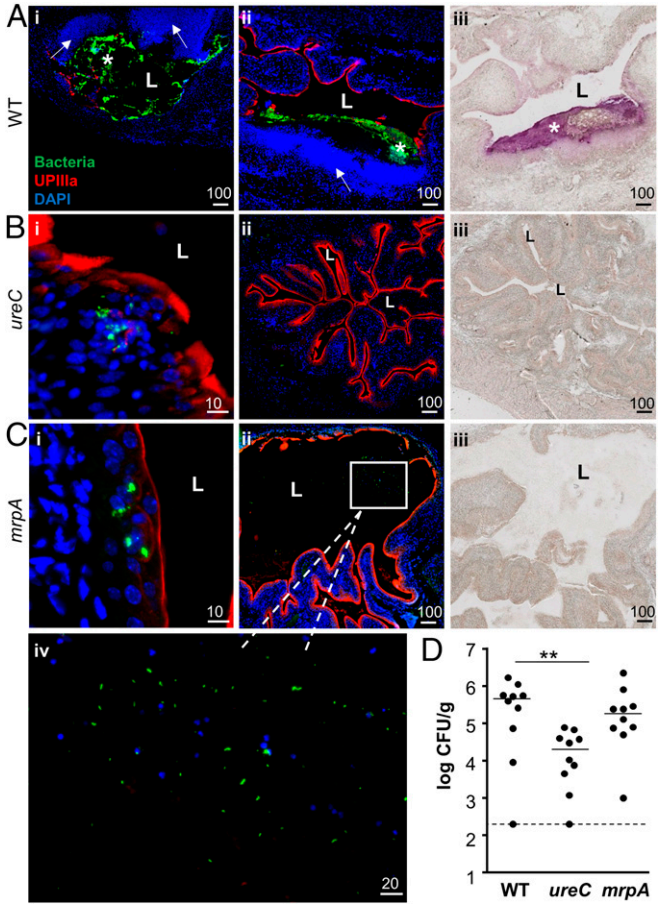

Fig. 4. *P. mirabilis mrpA* and *ureC* mutants are defective in cluster formation. (*A*–*C*) Representative sections of (*A*) *P. mirabilis* wild-type, (*B*) *ureC*, and (*C*) *mrpA*-infected murine bladders at 24 hpi. The wild-type–infected bladders show two regional views of clusters, whereas the mutant-infected bladders show a close-up of the urothelial surface (*B*, *i*; *C*, *i*] and a regional view (*B*, *ii*; *C*, *ii*). A region with a loose aggregate of *mrpA* mutant bacteria is boxed in *C*, *ii*, and magnified in *C*, *iv*. Bacteria are in green, UPIIIa in red, and DAPI in blue. (Scale bars, in micrometers, are as marked.) (*A*–*C*, *iii*) Alizarin Red staining of a section proximate to the regional view shown by immunofluorescent staining. Only wild-type *P. mirabilis*-infected bladders contain significant mineral deposition. L, bladder lumen; an asterisk indicates an extracellular cluster. Arrows indicate regions with increased DAPI signal. (*D*) Quantification of *P. mirabilis* wild type and mutant bladder colonization at 24 hpi. Dashed line indicates the limit of detection (200 cfu/g). $n = 10$ mice per strain tested.

maintenance of extracellular clusters as well as mineral deposition. We also compared the bacterial load of the *ureC* mutant to wild-type *P. mirabilis* at 24 hpi and found that the mutant had a 23-fold lower cfu/g than wild type (2.0×10^4 cfu/g tissue compared with 4.6×10^5 cfu/g tissue, respectively; $P = 0.0091$) (Fig. 4*D*). This is consistent with a previous study that reported a significant defect in bladder colonization at 48 hpi by the *ureC* mutant (11). In contrast, this mutant does not have an in vitro growth defect under a variety of culture conditions (Fig. S5). Overall, these data suggest that the *ureC* mutant is unable to thrive either intracellularly or extracellularly.

We also hypothesized that MR/P fimbriae might be important for cluster formation because they are essential for full bladder infection (4, 5), they are the most highly induced genes in bacteria isolated from the urine of infected mice at 24 hpi (28), and their expression in *P. mirabilis* or exogenously in *E. coli* results in autoaggregation (5, 6). Indeed, a *P. mirabilis mrpA* mutant failed to form typical extracellular clusters in murine bladders by 24 hpi. Instead, the bacteria were mostly in small intracellular groups (Fig. 4*C*, *i*). In one instance, we identified a loose Alizarin Red-negative luminal aggregation of the *mrpA* mutant embedded in a matrix of unknown material (Fig. 4*C*, *ii* and *iv*). Despite the distinct localization of *mrpA* mutant bacteria, the bladder cfu were not significantly different from wild type at 24 hpi (Fig. 4*D*; $P = 0.4813$).

Because urease activity of intracellular bacteria might be excluded from the bladder lumen, we tested the pH of urine from infected mice 24 hpi. We found modest increases in pH for both wild-type and *mrpA* mutant infected mice, although the increase was less for *mrpA* (Fig. S6). We did not see the massive infiltration that we found around wild-type clusters in bladders infected with either the *ureC* or *mrpA* mutant (Fig. 4 *A*–*C*, *ii*). Together, these data support a role for both urease and MR/P fimbriae in cluster formation and subsequent urolithiasis.

Discussion

To our knowledge, our study is the first to examine the localization of *P. mirabilis* in the bladder during the first 24 h after infection. Despite initially invading the urothelium (Fig. 5, 0.5 hpi), *P. mirabilis* primarily occupied an extracellular niche as infection proceeded (Fig. 5, 6 hpi). *P. mirabilis* formed large luminal clusters, dependent on both MR/P fimbriae and urease, which are likely precursors to urinary stones and resulted in extensive neutrophil recruitment (Fig. 5, 24 hpi). Clusters were nonuniform, and in addition to bacteria contained urothelial cell debris, mineral deposits, and neutrophils. This study, to our knowledge, is the first systematic characterization of the cellular localization of a uropathogen that engages in a life style distinct from that of UPEC.

What Is the Fate of Intracellular *P. mirabilis*? Previous studies showed that *P. mirabilis* is highly invasive in cultured cells (29, 30), and we found that *P. mirabilis* invaded the bladder epithelium as effectively as UPEC at 0.5 hpi (Fig. 1*E*; Fig. 5, 0.5 hpi). However, at later time points, intracellular *P. mirabilis* was primarily found as small and infrequent IBCs, suggesting that IBC development is not a key strategy for *P. mirabilis* (Fig. 5, 6–24 hpi). It is unclear why *P. mirabilis* largely fails to develop into IBCs. One possibility is that umbrella cells expel invaded *P. mirabilis* into the lumen, a phenomenon shown to occur during UPEC infection (31). *P. mirabilis* could be poorly adapted for an intracellular life style, resulting in host-mediated bacterial death. Alternatively, the invasive capacity of *P. mirabilis* and survival of the intracellularly located *mrpA* mutant suggest that the intracellular compartment could be an important component of infection, perhaps by modulation of the host response to extracellular bacteria.

Luminal Clusters Are an Essential Precursor to Urolithiasis. Our data suggest that extracellular clusters are an essential component of *P. mirabilis* infection: by 24 hpi, most bacteria were found in clusters that stained positive for mineral deposition (Fig. 2*D*; Fig. 4*A*; Fig. 5, 24 hpi). Based on this observation, we hypothesize that clusters correlate with urolithiasis and that bacteria themselves may be an essential component of urinary stones. Indeed, previous experiments showed that mature *P. mirabilis*-induced stones contain embedded bacteria and can serve as a reservoir for recurrent infections (8, 32, 33). We also note that clusters are not uniform in composition; although clusters may contain areas devoid of bacterial staining, these areas do not necessarily coincide with mineralization (note the serial sections in Fig. 4*A*, *ii* and *iii*). Important questions remain, including how frequently clusters develop into stones and which bacterial and host factors affect this process. Because extracellular clusters may mediate disease severity, it is imperative that future studies both identify the mechanism of their formation and determine whether this phenotype is prevalent in patients with *P. mirabilis*-dependent urolithiasis.

***P. mirabilis* Embedded in Extracellular Clusters Is Insulated from Neutrophil Attacks.** Clusters induce a rapid, extensive infiltration of neutrophils that, to our knowledge, is unlike any immune response reported in the literature (Fig. 3; Fig. 5, 24 hpi). Although the exact neutrophil staining pattern varied among clusters,

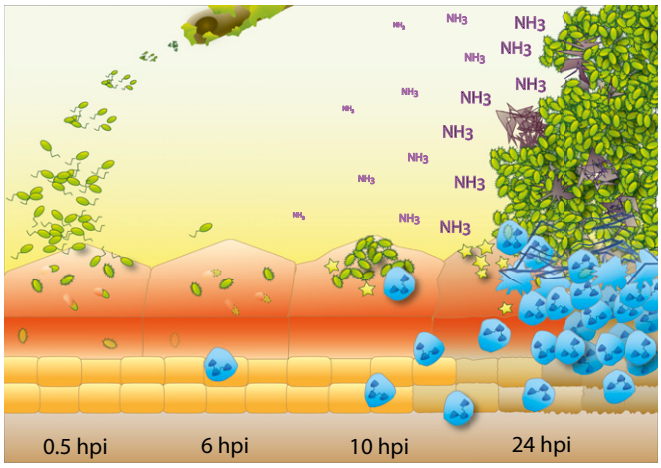

Fig. 5. Model of initial bladder colonization and cluster development by *P. mirabilis*. *P. mirabilis* infections are frequently associated with urinary catheters (*Top*). At early time points after gaining access to the bladder (0.5 hpi), bacteria (green) adhere to and invade urothelial umbrella cells; however, by 6 hpi, intracellular bacteria have largely disappeared (dashed outlining). Instead, fimbriated bacteria begin to form clusters on the apical surface of umbrella cells (10 hpi), which continue to grow (24 hpi), leading to increased local concentrations of toxins (yellow stars) and urease-generated ammonia (NH_3) as well as massive neutrophil infiltration (blue cells). The combined effect leads to crystalline mineral deposition (gray) and destruction of the urothelial surface.

we found recurring patterns of $Ly6G^+DAPI^+$, $Ly6G^+DAPI^-$, and $Ly6G^-DAPI^+$ staining. Upon closer examination, we identified instances of neutrophil attack on bacterial clusters via NETosis and phagocytosis. Indeed, a recent proteomic analysis suggested that NETs could occur specifically in response to *P. mirabilis*-mediated UTI (34). In addition to vital NETosis, regions with Ly6G staining but lacking nuclear DAPI signal may be the result of *P. mirabilis* toxins directly attacking infiltrating immune cells (35, 36). The potent immune response could be influenced by NLRP3-inflammasome activation; this pathway can be broadly activated by crystalline substances and specifically activated by *P. mirabilis* in the digestive tract (37, 38). It is also possible that neutrophils directly contribute to cluster formation, such as by providing materials for aggregation (i.e., DNA). Further studies of the immune response to *P. mirabilis* infection may examine the recruitment of additional innate immune effectors as well the mechanisms that *P. mirabilis* uses to evade immune cell attacks.

Both Urease and MR/P Fimbriae Are Essential for Extracellular Cluster Formation. There are several explanations for why the *ureC* mutant does not form clusters. In addition to causing mineral deposition, the generation of ammonia by urease also results in changes to the pH and nitrogen availability in the bladder lumen. Each of these aspects of urease activity could contribute to *P. mirabilis* adaptation to the harsh environment of the urinary tract, culminating in a defect for the *ureC* mutant in cluster formation or maintenance. Although the requirement of urease for stone formation has been known for decades (39), its necessity for cluster formation is a novel finding.

Although the importance of MR/P fimbriae in vivo is well established, the mechanism of MR/P contribution to virulence remains enigmatic. Previous in vitro studies support a role for MR/P fimbriae in autoaggregation (5, 6), hemagglutination (6, 40), and biofilm formation (5), phenotypes that are reminiscent of the in vivo clusters; indeed, we found that the *P. mirabilis mrpA* mutant failed to form extracellular clusters. We hypothesize that MR/P initiates cluster formation through interactions with the bladder surface, mineral deposits, other *P. mirabilis* cells, or, most likely, a combination of all of the above. The exact mechanism by which MR/P functions and identification of the binding target(s) remains an active area of investigation.

***mrpA* Mutant Persists in an Intracellular Niche.** Surprisingly, although the *mrpA* mutant failed to form luminal clusters, it may be more successful at surviving intracellularly than wild-type cells. However, other studies clearly show that *mrp* mutants are defective in colonization by 7 d postinfection (4, 6, 41, 42), indicating that the intracellular life style is not an effective long-term strategy for this pathogen. The intracellular phenotype of the *mrpA* mutant could be due to several factors, including altered attachment resulting in increased invasion or a different invasion pathway. In support of this, a previous study suggested that MR/P fimbriae affect the localization of bacteria in the bladder (5). Alternatively, the *mrpA* mutant may elicit an altered immune response or modify other host–pathogen interactions. It is also possible that a polar effect on the transcriptional regulator MrpJ, which is encoded in the *mrp* operon, and known to regulate an array of virulence-associated genes, contributes to the phenotypes of the *P. mirabilis mrpA* mutant (41). Thus, *mrpA* mutant phenotypes may be dependent on the fimbrial structure, on MrpJ targets, or both. Additional in vivo and in vitro studies will be needed to define the exact roles of MR/P fimbriae, particularly in attachment, invasion, and intracellular survival.

***P. mirabilis* and UPEC Occupy Distinct Locations in the Bladder.** In this and other studies, UPEC establishes an intracellular niche (Fig. 1*D*; Table 1). Others have reported UPEC in an adherent layer on the luminal surface or as filamentous bacteria extruding from urothelial cells (16, 43, 44). We found that, unlike UPEC, *P. mirabilis* primarily resided in large luminal clusters (Figs. 2*A* and 5; Table 1). Interestingly, cocolonization of *P. mirabilis* and UPEC results in increased UPEC bacterial loads in the bladder (45), which could be the result of *P. mirabilis* clusters and/or stones providing an additional niche for UPEC to colonize. Similarly, *P. mirabilis* cocolonization with *P. stuartii* results in increased *P. stuartii* bacterial loads compared with monospecies infection (46). These data emphasize the need to further investigate the life style of *P. mirabilis* and other understudied uropathogens, particularly in the context of polymicrobial infections.

Concluding Remarks. This study applied a technique commonly used to study UPEC pathogenesis to the understudied uropathogen *P. mirabilis*. We revealed that this pathogen uses a colonization pathway that is distinct from UPEC and results in a unique and robust immune response. By comparing colonization of wild-type and mutant *P. mirabilis*, we gained insight into the mechanisms of urease and MR/P contribution to virulence. These results provide a strong basis for future studies that will illuminate details of *P. mirabilis* invasion, life style, and interaction with the host that are essential for understanding and preventing *P. mirabilis* infection.

Materials and Methods

Bacterial Strains and Media. All bacterial strains were grown at 37 °C with aeration in low-salt LB (per liter: 10 g tryptone, 5 g yeast extract, 0.5 g NaCl) or on LB solidified with 1.5% agar. Antibiotics were added as needed: ampicillin (100 μg/mL) and kanamycin (25 μg/mL). The strains used in this study are in Table S1 and details on *mrpA* mutant construction are in *SI Materials and Methods*.

Mouse Model of UTI. Five- to seven-week-old female CBA/J mice (Jackson Laboratory) were infected with $1–2 \times 10^8$ cfu bacteria in PBS via transurethral catheter in accordance with New York University Langone Medical Center Institutional Animal Care and Use Committee-approved animal protocol 140204; details are in *SI Materials and Methods*.

Gentamicin Protection Invasion Assay. The ex vivo gentamicin protection assay was performed as previously described with the following modifications (14). At 0.5 hpi, infected bladders were aseptically extracted, bisected, and washed with PBS. One bladder half was incubated with DMEM + 100 μg/mL gentamicin and the other half with DMEM alone. Both halves were incubated at 37 °C for 1 h, washed with PBS, homogenized, serially diluted, and plated. Details are in *SI Materials and Methods*.

Immunofluorescence and Alizarin Red Staining. For immunofluorescence, 5-μm paraffin-embedded sections were processed and blocked, and antigens were detected with the appropriate primary and secondary antibodies and then

incubated with DAPI solution (Invitrogen). Sections were visualized on a Nikon TE2000 inverted microscope, and images were processed and pseudocolored using FIJI (47). To detect early stages of mineral deposition, we modified the Alizarin Red S staining procedure previously used to stain urinary stones caused by *P. mirabilis* (8). Detailed methods of staining, imaging, and measurement of IBC and cluster size are in *SI Materials and Methods*.

Statistical Analyses. To compare bacterial colonization, invasion, and IBC size, the nonparametric two-tailed Mann–Whitney test was used (GraphPad). Median values and statistical analyses with a P value ≤ 0.05 were reported. ($^{*}P \leq 0.05$, $^{**}P < 0.01$, $^{***}P < 0.001$).

ACKNOWLEDGMENTS. We thank Yi Liao, Xue-Ru Wu, Yan Liu, and Lisa Kuan for experimental advice and reagents and members of the New York University Urothelial Biology Group and the M.M.P. laboratory for stimulating discussion. This work was supported by National Institutes of Health (NIH) Grants AI083743 (to M.M.P.) and DK52206 and DK39753 (to T.-T.S.). The New York University Langone Medical Center Histopathology Core is partially supported by Perlmutter Cancer Center Grant P30CA016087 and NIH Grant UL1 TR00038.

1. Coker C, Poore CA, Li X, Mobley HLT (2000) Pathogenesis of *Proteus mirabilis* urinary tract infection. *Microbes Infect* 2(12):1497–1505.
2. Stickler DJ (2008) Bacterial biofilms in patients with indwelling urinary catheters. *Nat Clin Pract Urol* 5(11):598–608.
3. Schaffer JN, Pearson MM (2015) *Proteus mirabilis* and urinary tract infections. *Microbiol Spectr* 3(5):UTI-0017-2013.
4. Bahrani FK, et al. (1994) Construction of an MR/P fimbrial mutant of *Proteus mirabilis*: Role in virulence in a mouse model of ascending urinary tract infection. *Infect Immun* 62(8):3363–3371.
5. Jansen AM, Lockatell V, Johnson DE, Mobley HLT (2004) Mannose-resistant *Proteus*-like fimbriae are produced by most *Proteus mirabilis* strains infecting the urinary tract, dictate the in vivo localization of bacteria, and contribute to biofilm formation. *Infect Immun* 72(12):7294–7305.
6. Li X, Johnson DE, Mobley HLT (1999) Requirement of MrpH for mannose-resistant *Proteus*-like fimbria-mediated hemagglutination by *Proteus mirabilis*. *Infect Immun* 67(6):2822–2833.
7. Zhao H, Thompson RB, Lockatell V, Johnson DE, Mobley HLT (1998) Use of green fluorescent protein to assess urease gene expression by uropathogenic *Proteus mirabilis* during experimental ascending urinary tract infection. *Infect Immun* 66(1): 330–335.
8. Li X, et al. (2002) Visualization of *Proteus mirabilis* within the matrix of urease-induced bladder stones during experimental urinary tract infection. *Infect Immun* 70(1):389–394.
9. Jansen AM, Lockatell CV, Johnson DE, Mobley HLT (2003) Visualization of *Proteus mirabilis* morphotypes in the urinary tract: The elongated swarmer cell is rarely observed in ascending urinary tract infection. *Infect Immun* 71(6):3607–3613.
10. Mobley HLT, Island MD, Hausinger RP (1995) Molecular biology of microbial ureases. *Microbiol Rev* 59(3):451–480.
11. Johnson DE, et al. (1993) Contribution of *Proteus mirabilis* urease to persistence, urolithiasis, and acute pyelonephritis in a mouse model of ascending urinary tract infection. *Infect Immun* 61(7):2748–2754.
12. Zhou G, et al. (2001) Uroplakin Ia is the urothelial receptor for uropathogenic *Escherichia coli*: Evidence from in vitro FimH binding. *J Cell Sci* 114(Pt 22):4095–4103.
13. Wu XR, Kong XP, Pellicer A, Kreibich G, Sun TT (2009) Uroplakins in urothelial biology, function, and disease. *Kidney Int* 75(11):1153–1165.
14. Mulvey MA, et al. (1998) Induction and evasion of host defenses by type 1-piliated uropathogenic *Escherichia coli*. *Science* 282(5393):1494–1497.
15. Anderson GG, et al. (2003) Intracellular bacterial biofilm-like pods in urinary tract infections. *Science* 301(5629):105–107.
16. Mulvey MA, Schilling JD, Hultgren SJ (2001) Establishment of a persistent *Escherichia coli* reservoir during the acute phase of a bladder infection. *Infect Immun* 69(7): 4572–4579.
17. Lane MC, et al. (2005) Role of motility in the colonization of uropathogenic *Escherichia coli* in the urinary tract. *Infect Immun* 73(11):7644–7656.
18. Lloyd AL, Smith SN, Eaton KA, Mobley HLT (2009) Uropathogenic *Escherichia coli* suppresses the host inflammatory response via pathogenicity island genes *sisA* and *sisB*. *Infect Immun* 77(12):5322–5333.
19. Nielubowicz GR, Mobley HLT (2010) Host-pathogen interactions in urinary tract infection. *Nat Rev Urol* 7(8):430–441.
20. Daley JM, Thomay AA, Connolly MD, Reichner JS, Albina JE (2008) Use of Ly6G-specific monoclonal antibody to deplete neutrophils in mice. *J Leukoc Biol* 83(1):64–70.
21. Liu Y, El-Achkar TM, Wu XR (2012) Tamm-Horsfall protein regulates circulating and renal cytokines by affecting glomerular filtration rate and acting as a urinary cytokine trap. *J Biol Chem* 287(20):16365–16378.
22. Brinkmann V, et al. (2004) Neutrophil extracellular traps kill bacteria. *Science* 303(5663): 1532–1535.
23. Urban CF, et al. (2009) Neutrophil extracellular traps contain calprotectin, a cytosolic protein complex involved in host defense against *Candida albicans*. *PLoS Pathog* 5(10):e1000639.
24. Pilsczek FH, et al. (2010) A novel mechanism of rapid nuclear neutrophil extracellular trap formation in response to *Staphylococcus aureus*. *J Immunol* 185(12):7413–7425.
25. Yipp BG, et al. (2012) Infection-induced NETosis is a dynamic process involving neutrophil multitasking in vivo. *Nat Med* 18(9):1386–1393.
26. Mora-Bau G, et al. (2015) Macrophages subvert adaptive immunity to urinary tract infection. *PLoS Pathog* 11(7):e1005044.
27. Haraoka M, et al. (1999) Neutrophil recruitment and resistance to urinary tract infection. *J Infect Dis* 180(4):1220–1229.
28. Pearson MM, Yep A, Smith SN, Mobley HLT (2011) Transcriptome of *Proteus mirabilis* in the murine urinary tract: Virulence and nitrogen assimilation gene expression. *Infect Immun* 79(7):2619–2631.
29. Alamuri P, et al. (2010) Adhesion, invasion, and agglutination mediated by two trimeric autotransporters in the human uropathogen *Proteus mirabilis*. *Infect Immun* 78(11):4882–4894.
30. Chippendale GR, Warren JW, Trifillis AL, Mobley HLT (1994) Internalization of *Proteus mirabilis* by human renal epithelial cells. *Infect Immun* 62(8):3115–3121.
31. Miao Y, Li G, Zhang X, Xu H, Abraham SN (2015) A TRP channel senses lysosome neutralization by pathogens to trigger their expulsion. *Cell* 161(6):1306–1319.
32. Sabbuba NA, Mahenthiralingam E, Stickler DJ (2003) Molecular epidemiology of *Proteus mirabilis* infections of the catheterized urinary tract. *J Clin Microbiol* 41(11): 4961–4965.
33. Sabbuba NA, et al. (2004) Genotyping demonstrates that the strains of *Proteus mirabilis* from bladder stones and catheter encrustations of patients undergoing long-term bladder catheterization are identical. *J Urol* 171(5):1925–1928.
34. Yu Y, et al. (2015) Diagnosing inflammation and infection in the urinary system via proteomics. *J Transl Med* 13:111.
35. Swihart KG, Welch RA (1990) Cytotoxic activity of the *Proteus* hemolysin HpmA. *Infect Immun* 58(6):1861–1869.
36. Alamuri P, Mobley HLT (2008) A novel autotransporter of uropathogenic *Proteus mirabilis* is both a cytotoxin and an agglutinin. *Mol Microbiol* 68(4):997–1017.
37. Seo SU, et al. (2015) Distinct commensals induce interleukin-1β via NLRP3 inflammasome in inflammatory monocytes to promote intestinal inflammation in response to injury. *Immunity* 42(4):744–755.
38. Ciraci C, Janczy JR, Sutterwala FS, Cassel SL (2012) Control of innate and adaptive immunity by the inflammasome. *Microbes Infect* 14(14):1263–1270.
39. Griffith DP, Musher DM, Itin C (1976) Urease. The primary cause of infection-induced urinary stones. *Invest Urol* 13(5):346–350.
40. Bahrani FK, Mobley HLT (1993) *Proteus mirabilis* MR/P fimbriae: Molecular cloning, expression, and nucleotide sequence of the major fimbrial subunit gene. *J Bacteriol* 175(2):457–464.
41. Bode NJ, et al. (2015) Transcriptional analysis of the MrpJ network: Modulation of diverse virulence-associated genes and direct regulation of *mrp* fimbrial and *flhDC* flagellar operons in *Proteus mirabilis*. *Infect Immun* 83(6):2542–2556.
42. Li X, Lockatell CV, Johnson DE, Mobley HLT (2002) Identification of MrpI as the sole recombinase that regulates the phase variation of MR/P fimbria, a bladder colonization factor of uropathogenic *Proteus mirabilis*. *Mol Microbiol* 45(3):865–874.
43. Dhakal BK, Kulesus RR, Mulvey MA (2008) Mechanisms and consequences of bladder cell invasion by uropathogenic Escherichia coli. *Eur J Clin Invest* 38(Suppl 2):2–11.
44. Justice SS, et al. (2004) Differentiation and developmental pathways of uropathogenic *Escherichia coli* in urinary tract pathogenesis. *Proc Natl Acad Sci USA* 101(5): 1333–1338.
45. Alteri CJ, Himpsl SD, Mobley HLT (2015) Preferential use of central metabolism *in vivo* reveals a nutritional basis for polymicrobial infection. *PLoS Pathog* 11(1):e1004601.
46. Armbruster CE, Smith SN, Yep A, Mobley HLT (2014) Increased incidence of urolithiasis and bacteremia during *Proteus mirabilis* and *Providencia stuartii* coinfection due to synergistic induction of urease activity. *J Infect Dis* 209(10):1524–1532.
47. Schindelin J, et al. (2012) Fiji: An open-source platform for biological-image analysis. *Nat Methods* 9(7):676–682.
48. Hagberg L, et al. (1983) Ascending, unobstructed urinary tract infection in mice caused by pyelonephritogenic *Escherichia coli* of human origin. *Infect Immun* 40(1):273–283.
49. Liang FX, et al. (2001) Organization of uroplakin subunits: Transmembrane topology, pair formation and plaque composition. *Biochem J* 355(Pt 1):13–18.
50. Rigueur D, Lyons KM (2014) Whole-mount skeletal staining. *Methods Mol Biol* 1130:113–121.
51. Pearson MM, Mobley HLT (2007) The type III secretion system of *Proteus mirabilis* HI4320 does not contribute to virulence in the mouse model of ascending urinary tract infection. *J Med Microbiol* 56(Pt 10):1277–1283.
52. Belas R, Erskine D, Flaherty D (1991) Transposon mutagenesis in Proteus mirabilis. *J Bacteriol* 173(19):6289–6293.
53. Jones BD, Lockatell CV, Johnson DE, Warren JW, Mobley HLT (1990) Construction of a urease-negative mutant of *Proteus mirabilis*: Analysis of virulence in a mouse model of ascending urinary tract infection. *Infect Immun* 58(4):1120–1123.
54. Mobley HLT, Warren JW (1987) Urease-positive bacteriuria and obstruction of long-term urinary catheters. *J Clin Microbiol* 25(11):2216–2217.